

## Observations of atmosphere–ocean coupling in midlatitude western boundary currents

Kathryn A. Kelly, Michael J. Caruso, and Sandipa Singh

Physical Oceanography Department, Woods Hole Oceanographic Institution, Woods Hole Massachusetts

Bo Qiu

Department of Oceanography, University of Hawaii at Manoa, Honolulu

**Abstract.** Oceanographic fields derived from the Geosat altimeter and atmospheric fields from the European Centre for Medium-Range Weather Forecasts (ECMWF) were examined for both the western North Pacific Ocean and the western North Atlantic Ocean to determine the nature of the coupling. Despite the short data records, approximately 2.5 years, correlation analyses of nonseasonal fluctuations showed similar relationships for both oceans. Correlations between the height difference across the jets (surface transport) and the path of the western boundary currents suggested that there is a structural change of the recirculation gyres, associated with a path change, with timescales of 5–9 months. Both wind stress and wind stress curl were clearly correlated with the surface transport and path in each ocean. Although net surface heat flux and wind stress were correlated, there was no clear correlation between net surface heat flux from ECMWF and surface transport over the entire study region. Additional regional analyses of the North Atlantic showed a consistent relationship between cooling, sea surface temperature (SST), and surface transport west of 62°W; anomalous cooling (accompanied by cyclonic wind anomalies) corresponds to a weaker SST gradient across the Gulf Stream and decreasing surface transport. Because the surface transport fluctuations to the west and east of 62°W in the western North Atlantic are not correlated, structural changes in the recirculation gyres, which have their maximum variations east of 62°W, may not be related to surface heat flux variations.

### 1. Introduction

Observations of fluctuations in the surface transport and path of the Gulf Stream (GS) [Kelly, 1991] and the Kuroshio Extension (KE) [Qiu *et al.*, 1991] from 2.5 years of Geosat altimetric height data suggested similar large-scale patterns for both oceans: larger eastward surface transports corresponding to more northerly paths in the region of recirculation gyres. Two candidates for forcing such fluctuations are surface heat fluxes and wind stress. Large oceanic heat losses in winter are observed over both the KE and the GS regions [Isemer and Hasse, 1987; Hsiung, 1985]. To explain an observed April maximum in GS volume transport and path, Worthington [1976] postulated an “anticyclogenesis” model for the southern recirculation gyre in which the thermocline deepens during the winter in response to cooling by the atmosphere. The role of heat flux in driving ocean circulation was reexamined by *Cushman-*

*Roisin* [1987], who argued that the recirculation gyres held GS waters until surface heat fluxes could adjust the potential vorticity to that required for the water to reenter the ocean interior. *Huang* [1990] used an analytical model to show that atmospheric cooling could cause an intensification of the eastward flow and create northern and southern recirculation gyres. *Behringer et al.* [1979] noted that the warm core of the GS could amplify the effect of the local wind stress by increasing the drag coefficient. In addition, an analysis of the Geosat altimeter data by *Wunsch* [1991] showed strong correlations between the local wind stress and sea surface height (SSH) fluctuations; however, it is not clear whether the fluctuations in the eastward transport of the western boundary currents are equivalent to the basin-scale fluctuations observed by Wunsch. A complicating factor in examining the atmosphere–ocean coupling is the expected high correlation of wind and heat flux fields with each other [Cayan, 1992].

The path of the boundary current jet represents another aspect of the atmosphere–ocean coupling. The long-term mean location of both the KE and the GS coincides roughly with the line of zero wind stress curl, and fluctuations may also be correlated [Liu and Yang,

1994]. However, because of the correlation between path and transport seen in the altimetric data, it may be difficult to distinguish path and transport correlations with the wind field. There are some other possible sources of fluctuations in the path or transport, which are beyond the scope of this work. *Thompson and Schmitz* [1989] demonstrated that the addition of a deep western boundary current in a numerical model gave a more realistic mean GS path than wind forcing or topographic steering alone. Also, the path of the KE, in particular, may be sensitive to the upstream path of the Kuroshio, which attained both its straight and large-meander paths during the period [*Qiu*, 1992]. Finally, fluctuations in the surface transport may be due to eddy-mean flow interactions in the western boundary current itself [*Qiu*, 1995].

The large-areal coverage of ocean observations from satellites and the improved atmospheric fields from general circulation models (GCMs) allow a detailed investigation of the coupling between oceanographic and meteorological variables. This study examines the atmosphere-ocean coupling mechanisms through statistical analyses of the fields. The analysis is limited by the short data records from Geosat but has the advantage of having several simultaneous synoptic data sets. Section 2 is a description of the processing steps for the data, and section 3 describes the analyses performed on the data. A discussion of the results is contained in section 4, followed by the conclusions in section 5. The appendix contains a description of canonical correlations as used here.

## 2. Data Fields

Collinear height profiles for the 2.5-year Geosat Exact Repeat Mission (ERM) (November 1986 to April 1989) were processed using programs described by *Caruso et al.* [1990] to obtain a series of residual SSH. The mean SSH was estimated using the method of *Kelly and Gille* [1990], as modified by *Qiu et al.* [1991]. The estimate of the mean SSH was combined with the residual SSH to produce profiles of total SSH. Time series of the jet path and surface transport (height difference across the jet) were obtained from altimeter data for both the GS and the KE by fitting an error function across the eastward flowing current. Time series of height difference across the core of the jet were used in place of gridded SSH fields to separate the effects of current intensity from changes in the path. The height difference across the jet, unlike velocity, does not depend on the orientation of the jet with respect to the satellite subtrack. In addition, because the height difference is centered on the jet location in "stream coordinates" it is also independent of meridional path changes. Although the mean SSH was subsequently removed from the surface transport and path time series, it was an essential part of the analysis, in that it allowed us to locate the center of the jet. It also allowed us to distinguish the jet from rings and to isolate changes in jet strength from SSH fluctuations due to meandering.

Wind stress fields were derived from the  $2.5^\circ \times 2.5^\circ$  European Centre for Medium-Range Weather Forecasts (ECMWF) 1000-mbar, twice-daily model winds for October 1986 – December 1989. Winds were converted to wind stress using a wind-speed-dependent drag coefficient [*Large and Pond*, 1981] and were decimated to a semimonthly frequency. Some analyses of the 1000-mbar wind suggest that they are too strong and may produce stresses in error by as much as 50% [*Mestas-Nuñez et al.*, 1994]. This may enhance strong wind events relative to weaker fluctuations and somewhat alter the correlations; however, the errors in stress magnitude do not otherwise affect the results here.

Net ocean surface heat flux estimates were obtained from the ECMWF model for September 1986 – December 1989 on a  $1.125 \times 1.125^\circ$  grid for both oceans. Estimates of incoming shortwave radiation, outgoing infrared radiation, and latent and sensible surface heat fluxes, based on the accumulated values for two 6-hour periods per day, were modified as described by *Qiu and Kelly* [1993] to produce daily averages of net ocean surface heat flux, which were then decimated to a semimonthly frequency.

Two additional fields were available for the North Atlantic only. Sea surface temperature (SST) data from the advanced very high resolution radiometer (AVHRR) was processed as described by *Kelly and Qiu* [1995a] to obtain biweekly averages. An additional estimate of the net surface heat flux was obtained by assimilating temperature tendency into a mixed layer model [*Kelly and Qiu*, 1995ab] (hereinafter referred to as KQa and KQb, respectively).

The mean annual variations were removed from all of the variables, in order to examine the correlations of the nonseasonal signals. While important physically, the annual signal obscures statistical analyses because all inphase annual signals of the variables are correlated, regardless of any dynamical connection. Signals in quadrature will not contribute to these correlations. The latter is the expected dominant relationship between, for example, SST and heat flux; that is, one expects a relationship of the form  $\partial T / \partial t = Q$ , where  $T$  is SST and  $Q$  is the surface flux [*Cayan*, 1992]. The annual signal in wind stress, net surface surface heat flux, and SST was removed by least squares fits to the annual and semiannual harmonics at each grid point. Only the harmonics which accounted for at least 10% of the remaining data variance were removed, which meant generally that only the first harmonics were removed. For the jet path and transport the harmonics were removed from the original profiles for each satellite subtrack. After the annual signal was removed, the altimeter data were splined to a regular grid in increments of  $2^\circ$  longitude and the same semimonthly frequency as for the other variables. The annual signal accounted for only a relatively small amount of variance (9–12%) in the path and transport series, which represent the oceanic circulation. The amount of variance in the atmospheric fields was much larger, 22–56% in the wind stress components and 91–96% in the ECMWF surface flux fields.

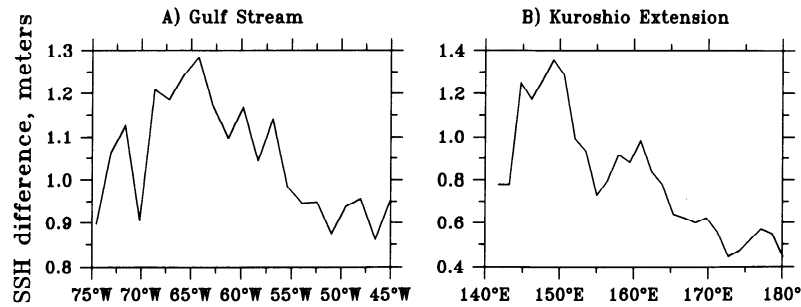


**Figure 1.** Mean surface transport from the Geosat altimeter. Temporally averaged sea surface height (SSH) difference for the (a) Gulf Stream (GS) and for the (b) Kuroshio Extension (KE). The height difference in the Gulf Stream at 70°W was underestimated by the method used to reconstruct the mean SSH from the altimetric data.

The annual signal was also the dominant component of North Atlantic SST, with 98% of the variance.

The mean surface transport (Figure 1) indicates the relative strength of the eastward flow in the boundary current; regions with large surface transport are regions of large recirculating flows. The KE has a local minimum in surface transport at 155°E (Figure 1b), which may indicate two regions of recirculation. At 70°W in the GS (Figure 1a) there is also a local minimum in surface transport, which is apparently an artifact of the method used to estimate the mean SSH difference. This minimum was erroneously attributed by Kelly [1991] to spatial structure in the recirculation gyre; however, additional analyses of the path fluctuations suggested that the jet did not meander enough for an estimate of the mean to converge properly. Although the standard deviation of the paths at 70°W formally met the criterion for convergence found by Qiu [1992], the distribution of paths was not Gaussian, and eliminating two outliers caused the path fluctuations to fail the criterion. None of the other subtracks in either the GS or the KE had this problem. The transports from this subtrack were included in the analyses here because the problematic temporal mean was removed.

Extrema of the ECMWF mean atmospheric fields (not shown) were generally north of the mean axis of the western boundary currents. The core of the westerlies in the North Atlantic is at the same latitude as the GS west of 60°W but is north of the GS to the east of 60°W. The core of the westerlies in the western North Pacific is everywhere north of the KE by at least 3° latitude. The mean wind is toward the northeast in both oceans. The minima of the mean net surface heat flux fields (maximum heat loss from the ocean) correspond to the longitude of maximum surface transport; however, the minimum heat flux in the Pacific, like the maximum wind speed, is displaced north of the KE, here by about 2–3° latitude.

All of the variables, with the annual signal removed, were subsequently low-passed filtered temporally with a half-power point of about six cycles per year. This removed approximately 50% of the remaining variance in the wind stress and 40% of the variance in the other variables for both the KE and the GS, except for the

KE path, for which the filtering removed only about 20% of the remaining variance.

### 3. Analyses of Nonseasonal Variations

The first step in the analysis was the computation of the time domain empirical orthogonal functions (EOFs) (see, for example, Davis, [1976]). The EOFs of the wind stress were computed using a complex variable for the  $x$  and  $y$  components, that is,  $\tau^x + i\tau^y$ . The fraction of variance in each of the first four EOFs for each variable is shown in Table 1, where variables in the western North Atlantic are designated by GS and those in the western North Pacific are designated by KE. The only variable which did not contain at least 40% of its variance in the lowest mode was SST (for the Atlantic). Surface heat flux has the largest amount of variance (>60%) in the first EOF. The KE path had about equal variance in its lowest two EOFs. In an analysis of the same data, Qiu *et al.* [1991] found similar modes and suggested that they represented propagation of the path fluctuations along the jet. This splitting of variance between two EOFs is not seen in the KE transport.

The coupling between the variables was determined using canonical correlation analysis, which is a decomposition of the data fields for two variables [Preisendorfer, 1988]. Canonical modes are analogous to EOFs for a single field in that the modes maximize the amount of cross-covariance between the two fields contained in the lowest modes, compared with maximizing the autocovariance of a single field in EOFs. A more detailed description of the procedure for computing the canonical modes is contained in the appendix. The canonical modes were computed from a truncated expansion in the EOFs of each variable using only the first four EOFs.

The canonical correlations give the covarying patterns and corresponding time series of the two fields; it is then necessary to evaluate the significance of the modes. For each canonical mode the correlation between the amplitudes of the time series for the two variables, the fraction of covariance explained, and an estimate of the correlation which would be significant at the 95% confidence level were computed. The num-

**Table 1.** Empirical Orthogonal Functions

Variable	Percent of Variance							
	Gulf Stream				Kuroshio Extension			
	1	2	3	4	1	2	3	4
Transport	54	17	14	10	43	23	13	10
Path	47	23	15	10	42	37	8.4	7.3
Wind stress	58	19	8.9	3.6	57	13	6.5	4.5
Surface heat flux	80	6.6	4.8	2.5	65	15	6.5	4.5
KQa surface flux	62	28	3.5	3.2				
SST	17	15	6.0	5.3				

Numbers 1–4 represent the first four EOFs in both regions. Gulf Stream is the western North Atlantic, Kuroshio Extension is the western North Pacific. KQa is *Kelly and Qiu* [1995a]. SST is sea surface temperature.

ber of degrees of freedom for each canonical analysis was estimated as the average of the degrees of freedom for the two variables. Only the statistics for those modes which had correlations above the estimated 95% confidence levels are shown in the tables below. As discussed by *Cayan* [1992], another test of the significance of the coupling of the fields is whether the lowest canonical modes correspond to the lowest EOFs of the two variables. Therefore, in each mode discussed below, the dominant EOFs for each variable in each canonical mode are listed in parentheses after the variable, in the order of their contribution to the canonical mode. For example, in Table 2 the first canonical mode of GS surface transport and path consisted primarily of the first EOF of transport and both the third and first EOFs of the GS path. The fraction of covariance described by this mode was 57%, with a correlation of 0.57, relative to a correlation of 0.43 required for a 95% level of confidence.

### Oceanographic Modes

The statistics of the canonical modes of surface transport and path fluctuations, which we will call “oceanographic modes,” are shown in Table 2. Both the first and second modes in the KE had statistically significant correlations; however, the first mode has a substantially larger amount of the covariance and represents lower transport and path EOFs, which contribute more to the variance of the fields. Only the first canonical mode in the GS was significant.

The first canonical oceanographic modes (Figure 2), which describe about half of the covariance, are remarkably similar in both oceans. Both have relatively high frequency fluctuations, with periods of approximately 5–9 months, and similar spatial structure: maximum amplitudes of the transport and path modes are downstream from the maximum mean transport, which is at 64°W in the GS and at 149°E in the KE. There are also trends in the modes, of opposite signs, so that the KE is tending toward a maximum in transport and more northerly position, while the GS is tending toward a minimum in transport and a more southerly position. The canonical correlation analysis, as described in the appendix, does not use spatial information in the calculation of the modes, and thus the similarity in structure between path and transport reinforces the significance of the coupling. The similarity in spatial structure was not apparent in the second KE modes. The first correlated modes show more clearly the relationship described in the previous Geosat analyses by *Kelly* [1991] and *Qiu et al.* [1991]: positive anomalies in surface transport are correlated with more northerly paths. The first canonical modes of the Gulf Stream were previously discussed by *Kelly and Watts* [1994].

### Atmospheric Modes

One problem in distinguishing whether surface heat flux or wind stress is coupled with the nonseasonal fluctuations in recirculation is the possibility that the atmospheric fields are highly correlated with each other.

**Table 2.** Oceanographic Canonical Correlation Statistics

Field 1	Field 2	Covariance, %	Correlation	95% Level
GS transport (1)	path (3,1)	57	0.57	0.43
KE transport (1)	path (1,2)	50	0.61	0.56
KE transport (2)	path (2,1)	37	0.57	0.44

GS is the Gulf Stream, KE is the Kuroshio Extension. Numbers in parentheses are the dominant empirical orthogonal functions in the order of their contribution to the canonical mode. See text.

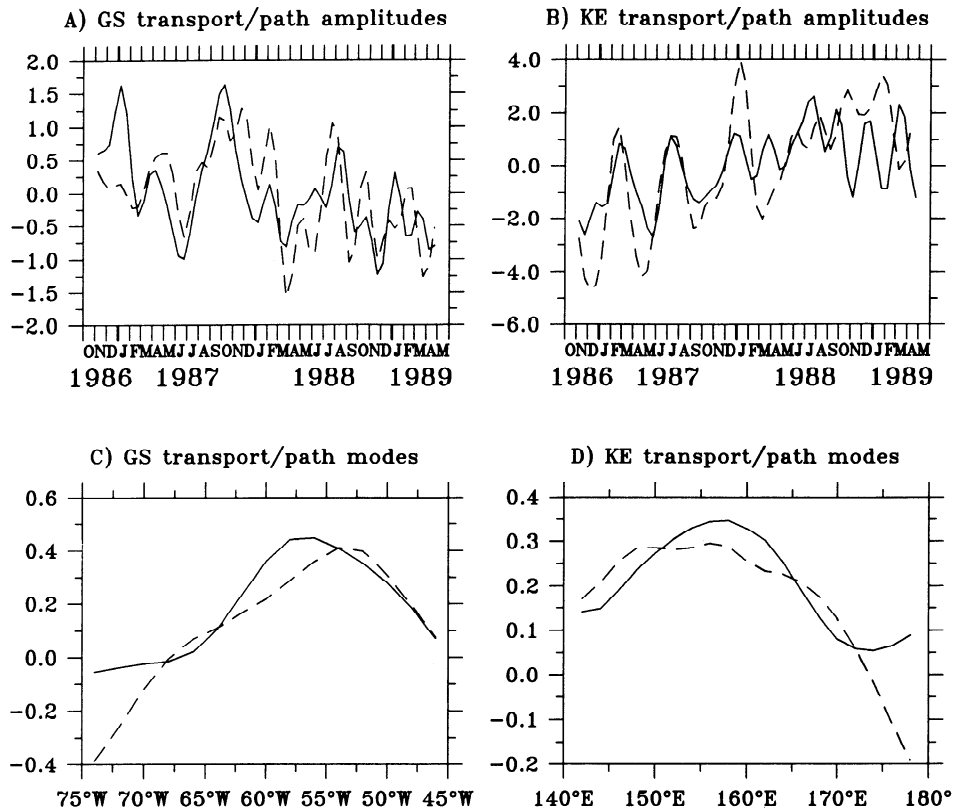


**Figure 2.** First canonical modes of transport and path. Time series for transport (solid line) and path (dashed line) for (a) Gulf Stream and (b) the Kuroshio Extension. Spatial modes of path (solid line) and transport (dashed line) for (c) Gulf Stream and (d) Kuroshio Extension. Note that the transport time series were increased by a factor of 2 for the GS and by a factor of 4 for the KE for plotting.

Thus we first examined the correlations between the atmospheric fields. The statistics of the canonical modes of wind stress and surface heat flux are shown in Table 3. Correlations for both oceans were clearly significant, with a high level (83%, 69%) of the covariance in the lowest modes. Correlations were larger for the North Atlantic than for the North Pacific.

The nature of the correlation between wind stress and surface heat flux (Figures 3 and 4) suggests a cooling response to increasing wind stress or cyclone activity. A positive value for the North Pacific flux mode (Figure 4c) in conjunction with the mean (not shown) gives higher wind speeds. According to *Cayan* [1992], there should be a negative surface heat flux anomaly (cooling) due to the higher wind speeds, which is what is shown by the surface flux mode (Figure 4b). A neg-

ative value of the North Atlantic mode (Figure 3c) in conjunction with the mean (not shown) also gives higher winds speeds over most of the region; however, the significance of this mode may be that the circulation of the negative anomaly is cyclonic, which is suggestive of a storm in the region. The corresponding surface flux anomaly is negative throughout the region, representing a loss of heat from the ocean.

**Wind Stress–Ocean Coupling**

The following two forms of coupling between the winds and the ocean were investigated: wind stress with surface transport and wind stress curl with the boundary current path. The statistics of the canonical modes for each boundary current are shown in Table 4.

**Table 3.** Atmospheric Canonical Correlation Statistics

Field 1	Field 2	Covariance, %	Correlation	95% Level
GS wind stress (1)	heat flux (1)	83	0.73	0.36
GS wind stress (2)	heat flux (2)	11	0.59	0.26
KE wind stress (1)	heat flux (1)	69	0.57	0.35
KE wind stress (3)	heat flux (2)	17	0.58	0.27

See Table 2 for description.

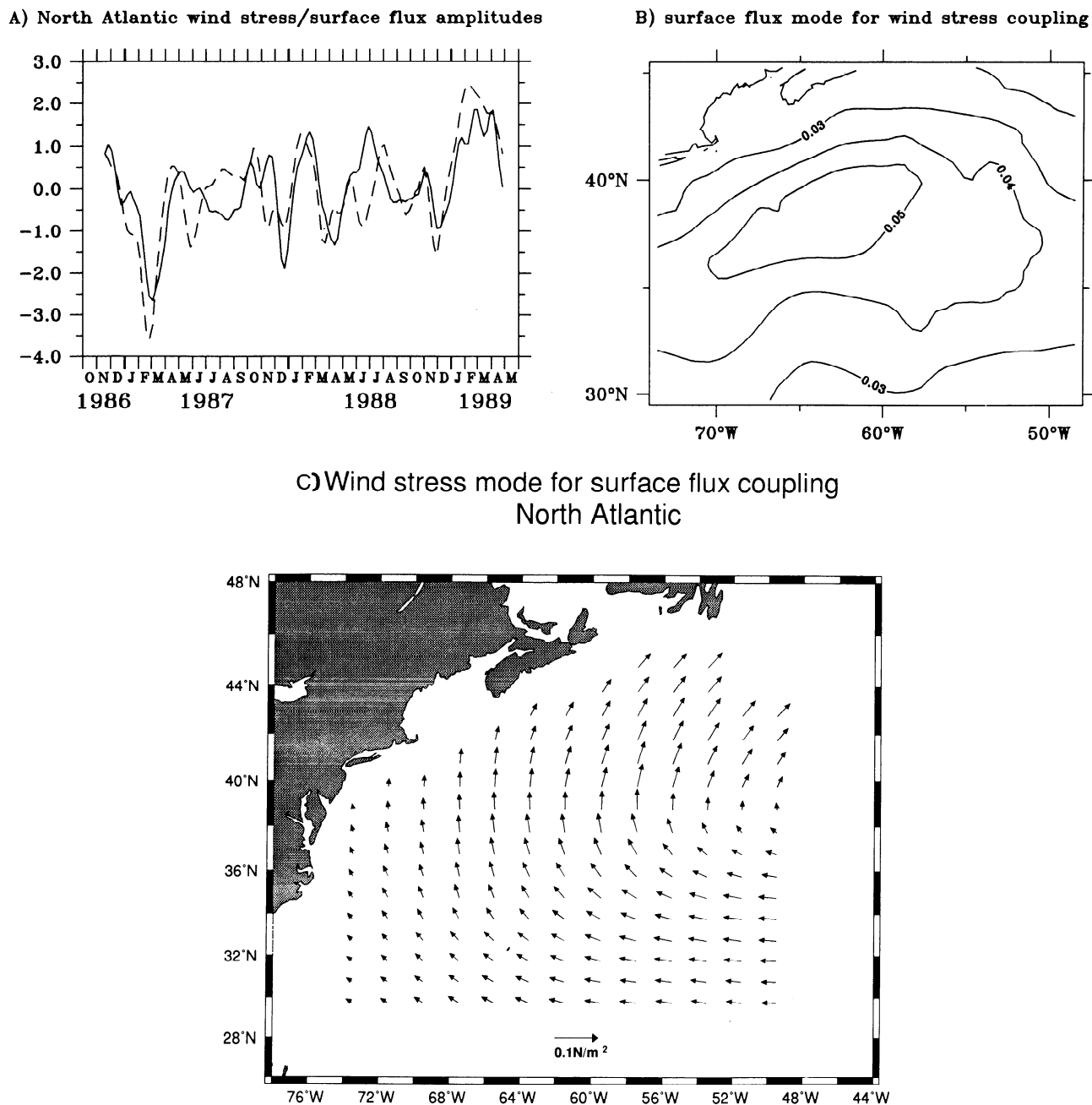
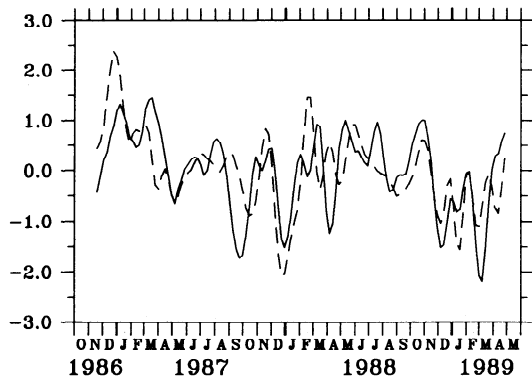


**Figure 3.** Canonical modes of wind stress and net surface heat flux for the North Atlantic. (a) Time series for wind stress (solid line) and surface flux (dashed line). Note that the surface flux time series has been reduced by a factor of  $10^3$  for plotting. Spatial modes of (b) surface flux and (c) wind stress.

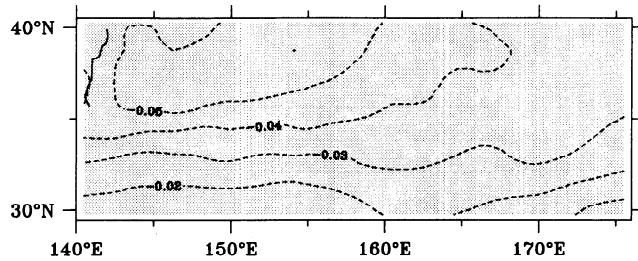
Two GS modes and one KE mode for the wind stress–transport analysis were statistically significant, although the correlations are not as high as those for the wind stress and the heat flux. The wind stress modes are linear combinations of the first and second EOFs of wind stress in the North Atlantic but only involve the second wind stress EOF in the North Pacific, so that the canonical modes represent substantially more wind stress variance in the Atlantic than in the Pacific. Regions of large wind stress anomalies generally correspond to regions of large transport anomalies. The first wind stress mode in the Atlantic (Figure 5e) is

virtually identical, with the reversed sign, to the wind stress–flux mode (Figure 3c); the corresponding transport mode has a negative anomaly in the west and a positive anomaly east of  $60^\circ\text{W}$  (Figure 5c). The second modes have the largest amplitudes east of  $60^\circ\text{W}$  for both the wind stress (Figure 5f) and the transport (Figure 5d). In the Pacific the wind stress has a large northward anomaly in the center of the region, near  $155^\circ\text{E}$  (Figure 6c), and the transport mode has a positive anomaly in the same region. However, there is also a negative transport anomaly near  $142^\circ\text{E}$ , with no corresponding corresponding wind stress anomaly.

A) North Pacific wind stress/surface flux amplitudes



B) surface flux mode for wind stress coupling



C) Wind stress mode for surface flux coupling North Pacific

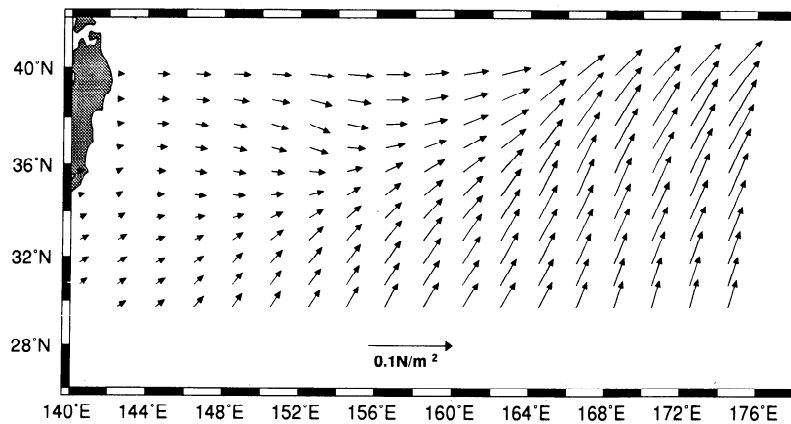


Figure 4. Same as Figure 3, but for North Pacific.

The statistics of the canonical modes of wind stress curl from ECMWF and path for each boundary current are also shown in Table 4. In the North Atlantic, the correlation is only with higher EOFs of path and curl; however, in the North Pacific there are two significant correlated modes which represent the lowest two EOFs of both fields. The first curl mode (Figure 7c) represents a southward shift of the westerlies in the vicinity of the KE, and the first path mode (Figure 7b) has a corresponding southward shift between about 150° and 180°E.

**Surface Heat Flux-Transport Modes**

The statistics of the canonical modes of net surface heat flux from ECMWF and surface transport for each boundary current region are shown in Table 5. Only one mode in each region was statistically significant, and neither canonical mode included the first EOF of heat flux. Again, the canonical correlations are not as high as in the atmospheric modes. The heat flux mode for the Atlantic (not shown) has its largest values in the western part of the region, whereas the transport mode

Table 4. Wind Stress-Transport Canonical Correlation Statistics

Field 1	Field 2	Covariance, %	Correlation	95% Level
GS wind stress (1,2)	transport (2)	47	0.42	0.39
GS wind stress (2,1)	transport (1)	44	0.39	0.35
KE wind stress (2)	transport (2,1)	35	0.52	0.37
GS curl (3,4)	path (3)	36	0.39	0.34
KE curl (1,2)	path (1)	57	0.57	0.44
KE curl (2)	path (2)	31	0.38	0.35

See Table 2 for description.

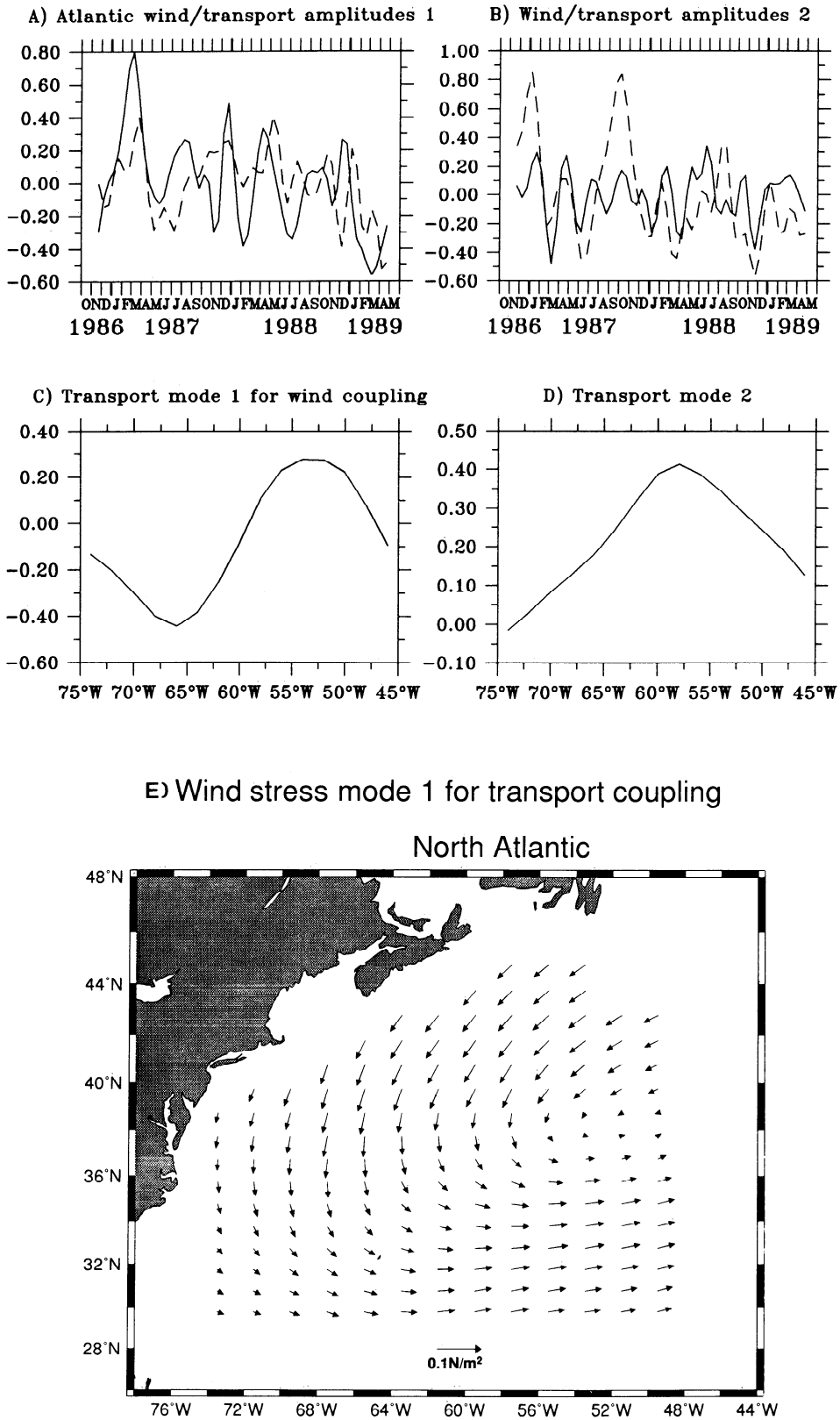


**Figure 5.** Canonical modes of wind stress and surface transport in the Gulf Stream. Time series for wind stress (solid line) and surface transport (dashed line) for (a) mode 1 and (b) mode 2. Note that the wind stress time series have been reduced by a factor of 3 for plotting. Spatial modes of surface transport for (c) mode 1 and (d) mode 2. Spatial modes of wind stress for (e) mode 1 and (f) mode 2.

F) Wind stress mode 2 for transport coupling

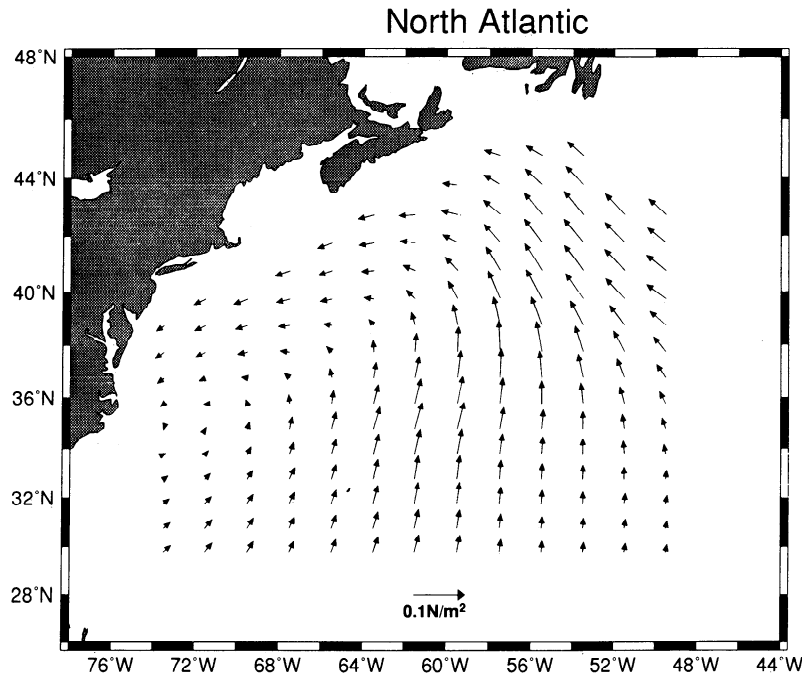


Figure 5. (continued)

has its largest values in the eastern part of the region. Although the Pacific (designated KE in Table 5) mode includes the second EOF of heat flux, this mode (not shown) probably reflects an artifact in the heat flux estimates, as discussed in section 4; the correlation is with the fourth EOF of transport.

KQa estimated the surface fluxes in the western North Atlantic for the same period by assimilating both altimetric SSH and temperature tendency from AVHRR data into a two-dimensional numerical mixed layer model. Although the spatially averaged surface flux estimate from this method agreed well with the ECMWF estimate,

there were considerable differences in the spatial structure. Canonical correlations between transport and the KQ surface flux estimate showed significant modes representing 55% and 14% of the covariance, respectively (Table 5). The first canonical mode consisted primarily of the second and first EOFs of surface flux, a substantially different result from the ECMWF analysis. The first KQ heat flux-transport modes (Figure 8) are more consistent than the ECMWF modes, in that both the flux and transport modes have their largest values in the eastern part of the region. The amplitudes of the modes show a trend from positive to negative values.

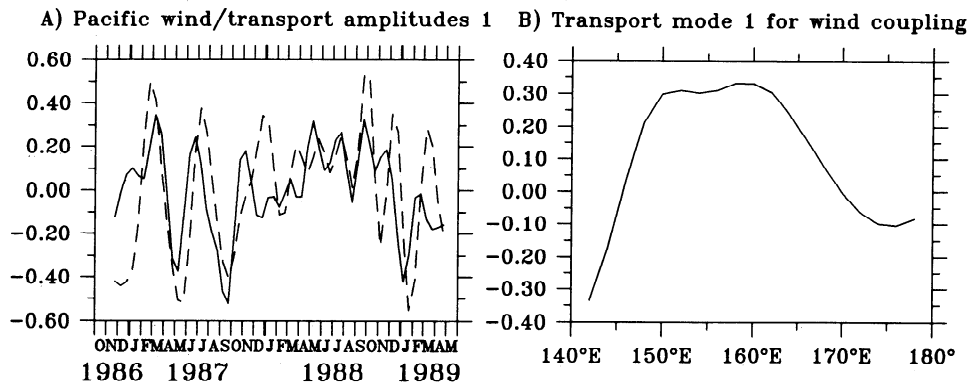


Figure 6. Canonical modes of wind stress and surface transport in the Kuroshio Extension. (a) Time series for wind stress (solid line) and surface transport (dashed line) for mode 1. Note that the wind stress time series has been reduced by a factor of 2 for plotting. (b) Spatial mode for surface transport, and (c) Spatial mode for wind stress.

CURRENTS

3



176°E

ation of the western bound-  
ge in structure in the recir-  
cale surface transport fluc-  
timeter were distinguished  
using the height difference  
ordinates. Fluctuations of  
ce transport were observed  
ths. These variations are



70°W



ension. (a) Time  
e that the wind  
Spatial mode for

**Table 5.** Surface Heat Flux Canonical Correlation Statistics

Field 1	Field 2	Covariance, %	Correlation	95% Level
GS surface flux (4,3)	transport (1)	27	0.48	0.45
KQ surface flux (2,1)	transport (1,2)	55	0.54	0.48
KQ surface flux (4,3)	transport (2,3)	14	0.63	0.38
KE surface flux (2)	transport (4)	22	0.48	0.37

See Table 2 for description.

more likely due to changes in the eastward flow of the recirculation gyres, which is as large as 150 Sv in this region, than to changes in the inflow, which is only about 50 Sv [Pierce and Joyce, 1988]. Consistent with this argument, the dominant transport modes in each boundary current have local maxima in the recirculation regions (Figure 2), at about 55–58°W in the GS and at about 154–160°E in the KE, whereas the magnitude of each mode is relatively small at the most upstream point. The fact that the maximum in transport fluctuations occurs downstream of the maximum mean transport suggests that there is an elongation/contraction of the recirculation gyre(s), rather than a change in the

strength of the recirculation. If the entire gyre were intensifying, one would expect maximum fluctuations where the mean flow is a maximum. These surface transport fluctuations are correlated with path changes, in that a more northerly path accompanies the elongation of the gyre.

To illustrate these fluctuations, SSH maps corresponding to both large and small values of the modes are shown for both the North Atlantic and the North Pacific (Figures 9 and 10). The extreme states of the SSH show the changes in the structure of the the recirculation gyre(s) between what we will call a “short gyre,” when the surface transport mode is negative, and an

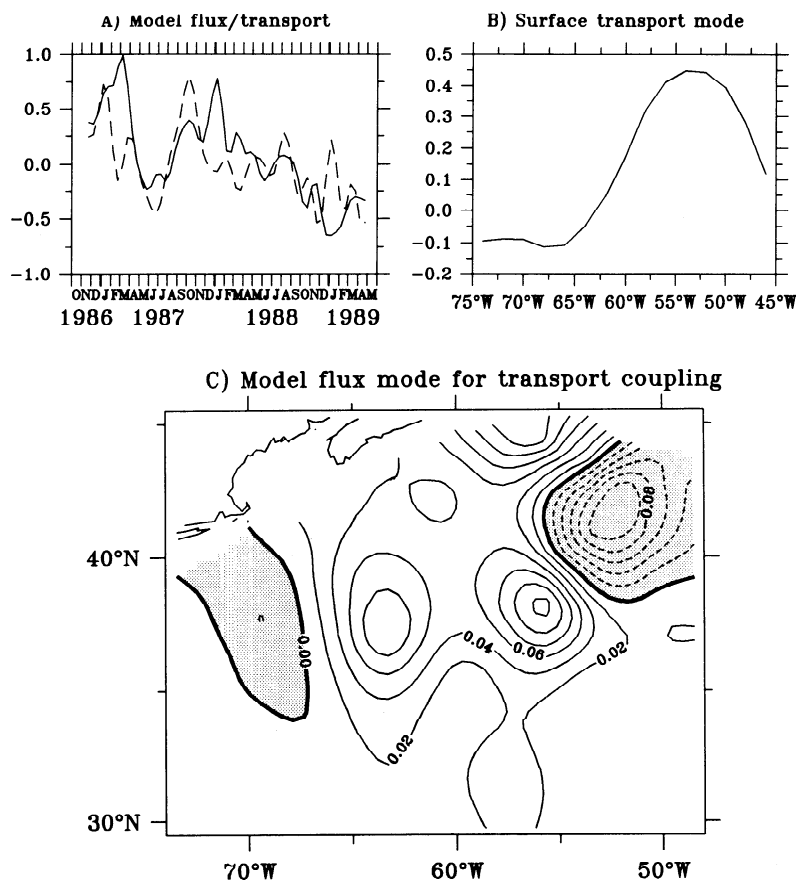


**Figure 8.** Canonical modes of net surface heat flux and surface transport in the Gulf Stream. (a) Time series for surface flux (solid line) and transport (dashed line) for mode 1. Note that the surface flux series was reduced by a factor of 2000 for plotting. (b) Spatial mode for transport, and (c) Spatial mode for surface flux (watts per square meter). The surface flux measurements used for these modes were derived by assimilating data into a mixed layer model.

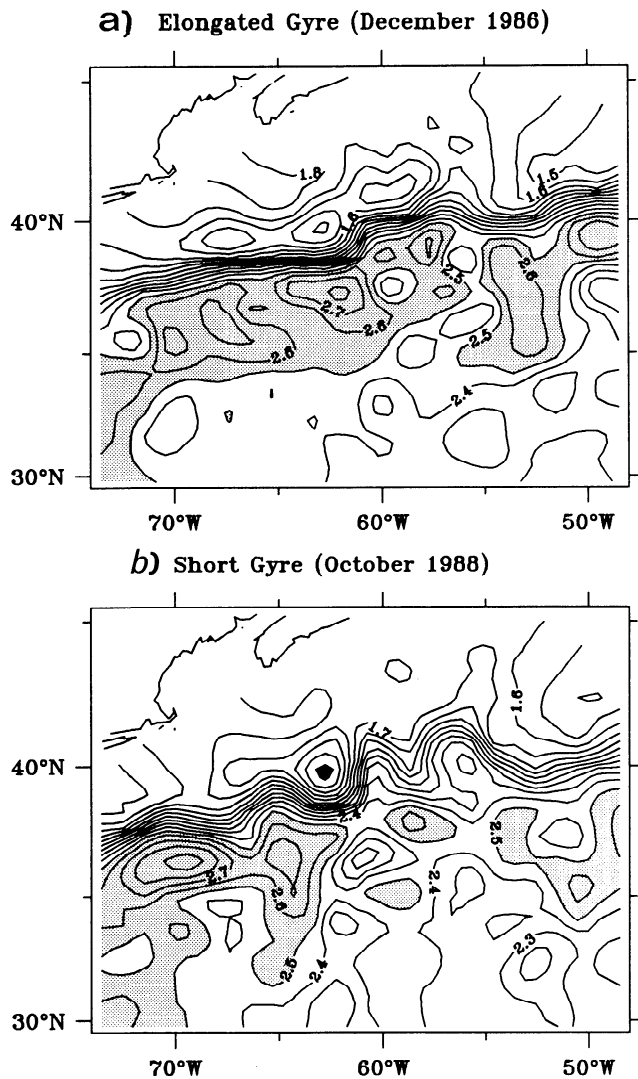


**Figure 9.** Changes in western North Atlantic surface geostrophic circulation. Maps of the sea surface height in the study area, averaged over 4 weeks, for (a) December 1986 and (b) October 1988. SSH anomalies larger than 2.5 m are stippled to highlight the changes in the recirculation gyre south of the Gulf Stream. Although these fluctuations represent extreme conditions over the 2.5-year period, there was a trend from an elongated recirculation gyre, as in Figure 9a, to a short gyre, as in Figure 9b.

“elongated gyre,” when the mode is positive. In the GS region there are changes in the structure of both the southern and the northern recirculation gyre (for a discussion of the northern gyre, see *Hogg et al.* [1986]). The changes in the southern recirculation gyre have been highlighted by shading in Figure 9. The changes in the gyres in the KE are less obvious (the southern circulation gyre has been shaded in Figure 10 also). However, a careful comparison of the number of contours in the jet between 155° and 160°E reveals a SSH difference for May 1987 that is nearly 0.2 m smaller than that for July 1988. Much of this difference appears to be due to differences in SSH on the northern side of the jet.

Although the changes in the recirculation gyres are apparent in the SSH maps themselves, the SSH maps were not used for the EOFs because fluctuations in SSH are dominated by smaller-scale changes in the position of the jet, primarily due to meanders. We chose instead to emphasize the large-scale fluctuations by using the stream coordinate variable, the SSH difference across the jet, centered on the location of the jet.

Fluctuations in the surface transport had statistically significant correlations with the lowest EOFs of the wind stress fields for both oceans (Table 4). In the Atlantic all of the first and second EOFs of each variable were represented in significant canonical modes. In the Pacific, only the second EOF of wind stress was represented in a significant canonical mode; however, the correlation was relatively high (Table 4). There were also significant coupled modes of wind stress curl and path for both oceans, although the coupling was stronger in the Pacific. The curl/path mode (Figure 7) was straightforward in the North Pacific: a more southerly path of the KE corresponded to a more southerly zero wind stress curl line. The meridional shifts in the North Pacific wind stress curl are likely related to changes in the meridional winds (Figure 6c), which are correlated with KE transport changes. Because surface transport and path are also significantly correlated (Table 2), we examined the canonical correlations between curl and KE transport and found one significant mode (correlation of 0.39, relative to a significance level of 0.33, for 35% of the covariance), which represented the second EOF of curl and the first and second EOFs of transport. This is a somewhat less significant result than the path correlation (0.57) and suggests that the curl may be more coupled with the path than with the transport in the North Pacific Ocean. Nevertheless, the high correlations between all the variables precludes a conclusive interpretation of the precise nature of the relationship between wind and ocean circulation.

Differences in the structure of the recirculation gyres due to changes in the wind field over the western boundary current were seen in the numerical simulations of *Rhines and Schopp* [1991]. Rhines and Schopp noted that the more zonally oriented North Pacific wind stress curl field produced an inertial jet that penetrated farther into the model interior (an elongated gyre) and that a curl field which had a southwest/northeast tilt in the zero curl line produced a jet with less penetration (a short gyre), similar to what is observed in the mean circulation in the North Atlantic. To see whether changes in the orientation of the curl field could be causing the GS transport fluctuations, we estimated the slope of the zero curl line in the Atlantic from the wind stress curl maps. We found no significant correlation between the gyre fluctuations and the nonseasonal curl line tilt on timescales of months. However, there was a trend over the 2.5-year period toward a more tilted curl line, which coincided with a trend toward a shorter recirculation gyre. However, it is impossible to establish such a relationship on this longer timescale with the present short data record.

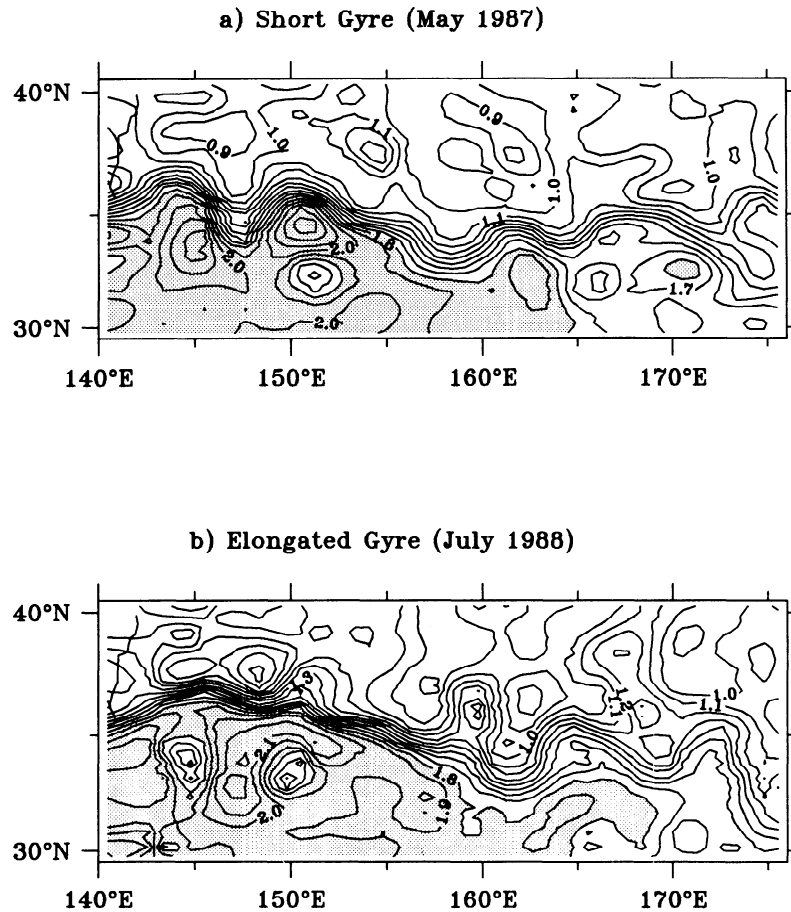


**Figure 10.** Changes in western North Pacific surface geostrophic circulation. Maps of the sea surface height in the study area, averaged over 4 weeks, for (a) May 1987 and (b) July 1988. SSH anomalies larger than 1.8 m are stippled to highlight the changes in the recirculation gyre south of the Kuroshio Extension. Although these fluctuations represent extreme conditions over the 2.5-year period, there was a trend from a short recirculation gyre, as in Figure 10a, to an elongated gyre, as in Figure 10b.

Correlations between the transport and surface heat flux fields from ECMWF showed significant correlations only for higher EOFs. In the Atlantic the significant mode consisted primarily of the fourth EOF of surface flux, which represents only 2.5% of the flux variance. In the Pacific the correlation is primarily with the second EOF of the surface flux, and this EOF may be spurious due to a problem in reconstructing the fluxes from the available ECMWF data. As discussed by *Qiu and Kelly* [1993], the available fluxes were the accumulated values over two 6-hour periods of each day, rather than a daily average. Because the same 6-hour periods, relative to UTC, were used globally, temporal variations in the estimates of incoming solar radiation were aliased into zonal variations in the heat flux estimates. Although *Qiu and Kelly* attempted to remove this artifact by modeling the diurnal variations of the incoming solar radiation, there was still a systematic zonal variation in the corrected data.

An alternative estimate of the net surface flux was available for the North Atlantic, derived from assimilating SST and altimetric velocity into a mixed layer

model (KQa). The analysis of the heat budget in the western North Atlantic (KQb) suggested that a trend in the estimated net surface heat flux was due to cooling by advection from Ekman transport; this trend was also observed in the ECMWF fluxes and can be seen here in the time series of the wind-heat flux coupled mode in Figure 3a. However, the effects of Ekman transport appear to have been exaggerated by the use of wind stress estimates that were too large, as noted in section 2. Because the heat flux was estimated as the residual of the mixed layer heat budget, errors in the calculated terms would cause errors in the flux estimates. A further complication in using this heat flux estimate is that geostrophic advection in this two-dimensional model was estimated from the same altimetric SSH fields used for this analysis. Thus, in some sense, changes in surface transport are incorporated in the KQ heat flux estimates. This effect, although not large, was discernible in the advection terms of the heat budget, as discussed in KQb.

Canonical correlations between surface transport and the KQ surface flux estimates showed two significant

modes, one (correlation of 0.54, relative to a significance level of 0.48, for 54% of the covariance) representing the lowest EOFs (Table 5), a substantially different result from the ECMWF analysis. The first heat flux mode (Figure 8c) shows a predominantly positive value corresponding to a positive value of surface transport downstream of 60°W. A physical interpretation of this result (using the negative amplitude) is that anomalous surface cooling weakens the temperature gradient across the GS, which in turn weakens the baroclinic flow through the thermal wind relationship and therefore decreases surface transport. However, there is also a large anomaly of the opposite sign centered on 52°W, 42°N (Figure 8c) in the region where the large Ekman transport created unrealistically large positive heat flux values (KQb). To check whether the higher correlation of the KQ flux and surface transport was due to the wind, we removed that part of the flux variations which was correlated with the wind and recalculated the correlation. To do this, we first found which of the EOFs were contributing the most to the canonical modes. The largest and only significant single correlation (−0.52, relative to a significance level of 0.41) of the individual EOFs was between the first EOF of transport and the second EOF of surface flux. We next computed the linear regression coefficients  $a_i$  between the second flux amplitude  $q_2$  and each wind stress amplitude  $\tau_i$

$$a_i = \frac{\langle q_2 \tau_i \rangle}{\langle \tau_i^2 \rangle}, \quad i = 1, 2 \quad (1)$$

and then subtracted to obtain the flux amplitude residual  $\tilde{q}_2$ ,

$$\tilde{q}_2 = q_2 - a_1 \tau_1 - a_2 \tau_2 \quad (2)$$

where angle brackets denote the expected value. The correlation between the residual flux amplitude  $\tilde{q}_2$  and the first transport mode was nearly the same (−0.51, relative to a significance level of 0.40). This suggests that there is a coupling between the transport fluctuations and the KQ surface flux, as derived from the mixed layer model, which is independent of (linear variations of) wind stress. The higher correlation with the KQ fluxes suggests that the ECMWF heat fluxes may lack the necessary spatial resolution for this analysis. This result should be viewed with caution, however, because of the use of the SSH in the mixed layer model.

For the North Atlantic we also analyzed SST, a frequently used variable in climatological studies of atmosphere-ocean interaction (e.g., Kushnir, 1994; Deser and Blackmon, 1993). Using the SST maps produced for the KQ analyses of the heat budget, we found a coupling of SST with wind stress and with surface transport. The first wind stress-SST mode has a correlation of 0.67, relative to a significance level of 0.39, for 81% of the covariance. This mode has a time series (Figure 11a) and a wind stress spatial mode (not shown) which strongly resemble the wind stress-surface flux (ECMWF) coupling (Figures 3a and 3c, respectively). This mode shows a decrease in the SST gradient across the GS (negative amplitude of the mode in Figure 11b)

corresponding to a cyclonic wind stress anomaly. The first mode (Figure 12b) of the canonical SST-transport has a correlation of 0.70, relative to a significance level of 0.45, for 46% of the covariance. This mode shows a decrease in the GS surface transport in the western part of the region and a strengthening in the eastern part, accompanied by a weakening of the SST gradient across the GS (Figure 12c). Combining the results of these highly coupled SST-wind-transport modes, we find a consistent picture of the GS response to wintertime storm conditions for the region west of about 60°W: cyclonic wind events correspond to a weakening of the SST gradient (cooling) and a weakening of the surface geostrophic current. The SST-transport coupling east of 60°W is less intuitive, in that it shows a warming of the slope water and a cooling of the GS water, accompanied by a larger surface transport.

If fluctuations in GS transport are due to surface heat flux, then one would expect anomalous cooling of the ocean to weaken the temperature gradients and the baroclinic flow field, consistent with the SST-transport modes west of about 60°W. To see whether the ECMWF fluxes agree with this model, spatially averaged values of the ECMWF heat flux were compared with spatially averaged values of surface transport west of about 60°W. The mean and annual signal were first removed from each time series, and a correlation (0.44) was found between them, which was not significant at the 95% level (approximately 0.53). However, if the height difference across the GS actually measures the heat content (difference), then the two time series should be phase-lagged; that is,  $\partial \Delta \eta / \partial t = Q$ , where  $\Delta \eta$  is the surface transport. For the region west of 62°W a positive correlation between these (nonseasonal) variables was found (0.52, relative to 0.45); that is, anomalous cooling produces a decreasing surface transport. Including surface transport fluctuations east of 62°W degraded the correlations. Because the correlated path-transport mode (Figure 2c) has its maximum amplitude east of 62°W, this simple response to cooling is not necessarily related to the recirculation gyre fluctuations (Figure 10).

According to the *Worthington* [1976] model, wintertime cooling should be accompanied by a steepening of the thermocline, which increases the strength of the recirculation gyre and therefore of the eastward GS volume transport. To be consistent with the relationships observed here, where surface transport weakens with anomalous cooling, the effects of seasonal heating/cooling would have to be relatively shallow, so that fluctuations in the thermocline would be anticorrelated with SSH fluctuations. This was not what was observed in a comparison between changes in surface transport and changes in the depth of the thermocline across the GS. Using measurements from inverted echo sounders (IESs) for the Synoptic Ocean Prediction program (SYNOP) in the GS, *Kelly and Watts* [1994] showed that the surface transport fluctuations at 68°W were positively correlated with transport fluctuations above the thermocline; that is, a larger surface transport was positively correlated with a larger transport

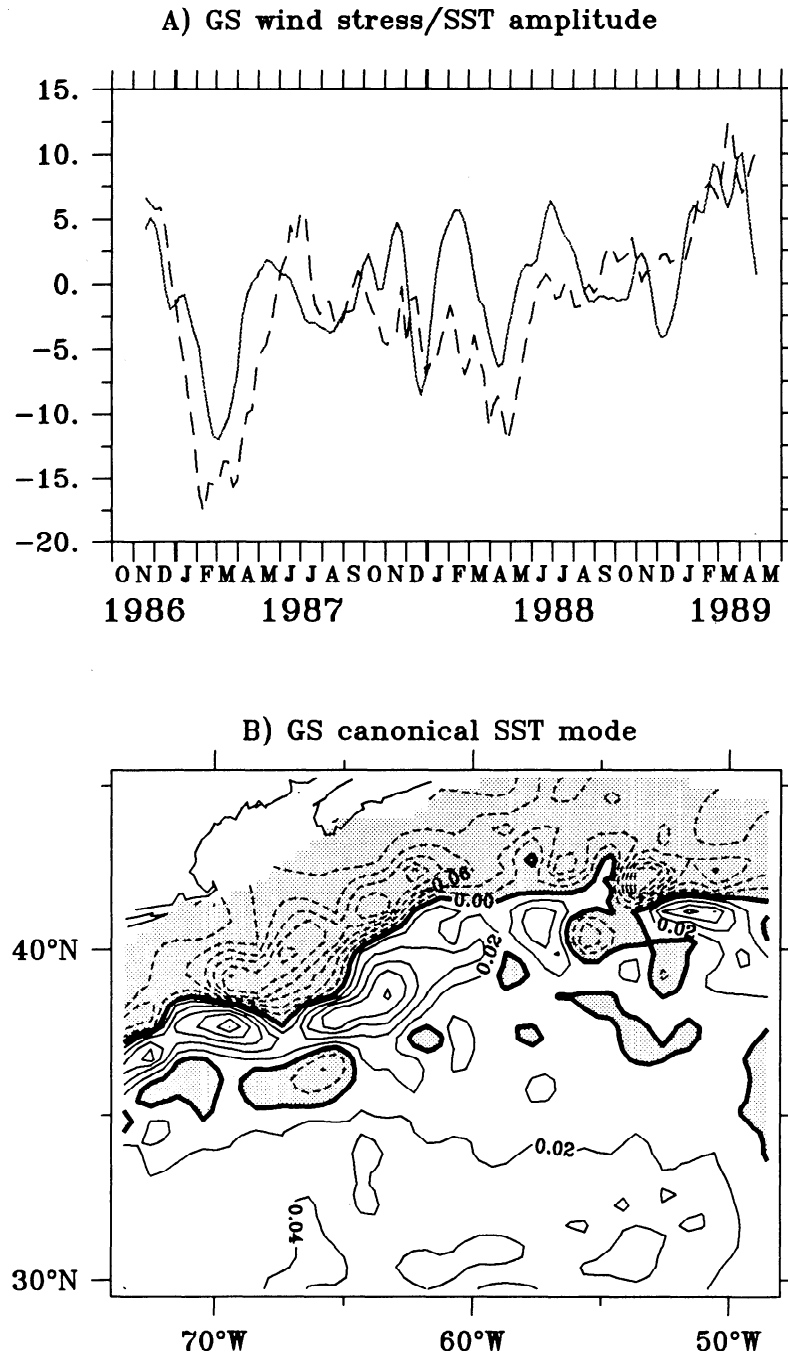


**Figure 11.** Canonical modes of wind stress and sea surface temperature (SST) for the North Atlantic. (a) Time series for wind stress (solid line) and SST (dashed line) for the Gulf Stream for mode 1 and (b) spatial mode of SST. Note that the wind stress time series was increased by a factor of 5 for plotting. The spatial mode of wind stress was nearly identical to the wind stress-surface flux mode in Figure 3c.

above the thermocline. This correlation may, however, reflect the importance of large meanders, which dominate the dynamics at this location, relative to the heating/cooling cycle. The fluctuations in surface transport at  $68^{\circ}\text{W}$  were as large as 0.60 m on timescales of a few weeks, in comparison with the fluctuations of less than 0.20 m here on timescales of several months. In the atmosphere-ocean coupling analysis here we attempted to filter out fluctuations with short spatial scales.

The statistical analysis does not yield a conclusive statement about the relevant mechanisms, particularly when several of the fields are highly correlated. What is clear from the analysis is that fluctuations in surface transport/path are correlated with fluctuations in the wind stress/curl in both oceans. In the North Atlantic west of  $62^{\circ}\text{W}$  there appears to be a consistent relationship between cooling, SST, and surface transport: anomalous cooling (accompanied by cyclonic wind

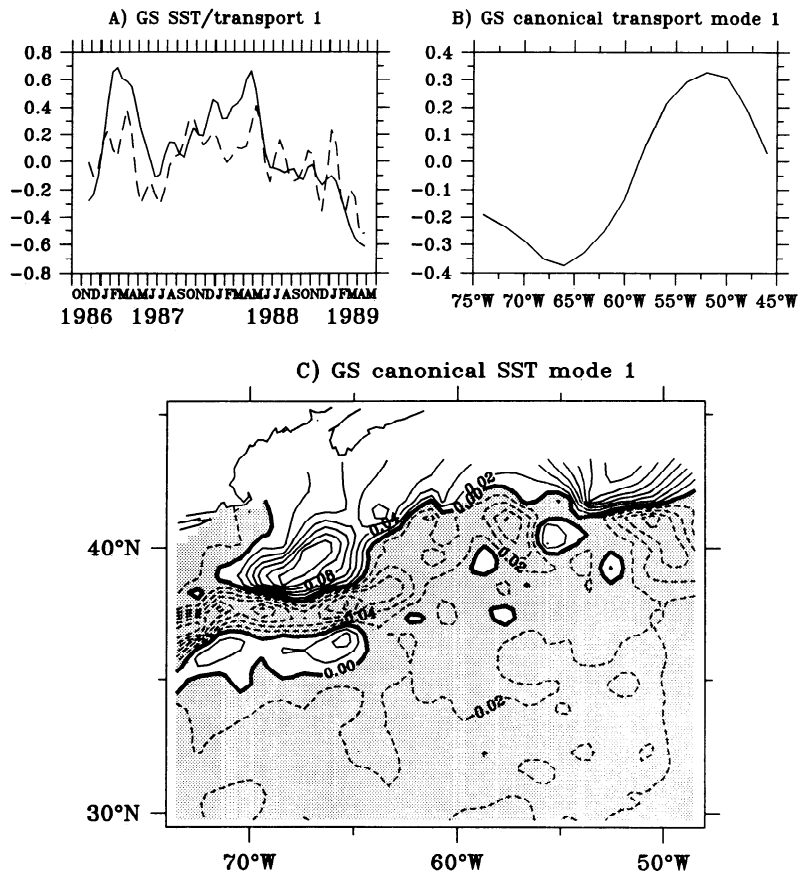


**Figure 12.** Canonical modes of SST and transport for the North Atlantic. (a) Time series for SST (solid line) and transport (dashed line) for the Gulf Stream for mode 1. Note that the SST time series was reduced by a factor of 20 for plotting. Spatial modes of (b) SST and (c) Transport.

anomalies) corresponds to a weaker SST gradient across the GS and weakening surface transport. Looking at the trends in the variables, one sees that the winter/spring of 1986–1987 was more severe than that of 1988–1989, with accompanying stronger (cyclonic) wind stress and more negative surface heat fluxes. Over this time period the KE strengthened and moved farther north. The GS appears to have done the opposite (weakened and moved farther south) over the same period. However, a closer examination reveals that while the recirculation gyre contracted (weaker surface transport in the eastern region), the surface transport in the western region became stronger (KQB, Figure 8). A longer time series is needed to allow resolution of these longer timescales. Longer and more accurate time series will be available in the future, in particular, from the TOPEX/POSEIDON altimeter.

## 5. Conclusions

Canonical correlation analyses were performed on oceanographic fields from the Geosat altimeter and atmospheric fields from the ECMWF for both the western North Atlantic and the western North Pacific Oceans. The analysis of the surface transport and the path of the western boundary currents suggested that the dom-

inant mode of variability in both oceans is a contraction and expansion of the recirculation gyres, which is associated with a large-scale path change, with periods of 5–9 months.

Fluctuations in the surface transport of the western boundary current were significantly correlated with wind stress fluctuations for both the Atlantic and the Pacific, whereas the correlations between transport and surface heat flux from ECMWF did not appear to be significant over the entire region in either ocean. There were also significant correlations of wind stress curl and the path of the eastward flowing current; however, the high correlations between all the variables preclude a conclusive interpretation of the nature of the wind stress–ocean circulation coupling.

Additional analyses in the North Atlantic showed differing results in the regions west and east of about 62°W. An alternative estimate of the surface flux for the North Atlantic was significantly correlated with the surface transport to the east of 62°W; however, this estimate may have its largest errors in this region. West of 62°W, a simple oceanic response to wintertime cooling was apparent: anomalously negative heat fluxes (accompanied by cyclonic winds) corresponded to a weaker SST gradient across the GS and decreasing surface transport. However, because the surface transport fluctu-

tuations east and west of 62°W are uncorrelated, this simple response is not necessarily related to the recirculation gyre fluctuations, which have their maximum variations east of 62°W.

## Appendix: Canonical Correlations

To compute the canonical modes, we start with the EOFs of each field, which was done using singular value decomposition (SVD) as in the work by Kelly [1988]. An  $M \times N$  data matrix  $\mathbf{D}$ , which contains in each row a time series of length  $N$  for  $M$  spatial points, is factored into orthogonal spatial functions  $\mathbf{U}$  by

$$\mathbf{D} = \mathbf{U}\mathbf{S}\mathbf{V}^T \quad (\text{A1})$$

where the superscript indicates the transpose of a matrix and the spatial modes are the columns of  $\mathbf{U}$ . The time-varying amplitudes of the spatial functions are the columns of  $\mathbf{A}$ , which is given by

$$\mathbf{A} = \mathbf{V}\mathbf{S}^T \quad (\text{A2})$$

where  $\mathbf{A}^T\mathbf{A} = \mathbf{I}$ . The number of functions is determined by  $P = \min(M, N)$ , and  $\mathbf{S}$  is an  $M \times N$  matrix, which contains a  $P \times P$  diagonal submatrix and the remainder consists of zeros. The eigenvalues in the usual formulation for EOFs are the squares the diagonal elements of  $\mathbf{S}$ , also known as the "singular" values.

After each field has been decomposed separately using SVD, an additional SVD decomposition is performed on the amplitude matrices of the two fields, which have been truncated to contain only those modes which described a significant portion of the data variance,

$$\mathbf{A}_1^T\mathbf{A}_2 = \mathbf{C}_1\mathbf{L}\mathbf{C}_2^T \quad (\text{A3})$$

These coefficient matrices  $\mathbf{C}_i$  are used to form the canonical modes,

$$\mathbf{F}_i = \mathbf{U}_i\mathbf{C}_i, \quad i = 1, 2 \quad (\text{A4})$$

which are simply linear combinations of the original functions  $\mathbf{U}_i$ . This relationship can be clarified by formulating the cross-covariance matrix,

$$\mathbf{D}_1\mathbf{D}_2^T = \mathbf{U}_1\mathbf{A}_1^T\mathbf{A}_2\mathbf{U}_2^T \quad (\text{A5})$$

which, using the decomposition (A3) becomes

$$\mathbf{D}_1\mathbf{D}_2^T = \mathbf{U}_1\mathbf{C}_1\mathbf{L}\mathbf{C}_2^T\mathbf{U}_2^T = \mathbf{F}_1\mathbf{L}\mathbf{F}_2^T \quad (\text{A6})$$

Thus the covariance has been factored into the canonical modes  $\mathbf{F}_i$ , with the diagonal matrix  $\mathbf{L}$  giving the relative contribution of each canonical mode to the covariance. The amplitudes  $\mathbf{B}_i$  of these canonical modes are given by

$$\mathbf{B}_i = \mathbf{A}_i\mathbf{C}_i \quad (\text{A7})$$

The correlation and its statistical significance for each canonical mode is computed from the amplitudes  $\mathbf{B}_i$  for each mode.

**Acknowledgments.** The authors gratefully acknowledge the support of the Mellon Joint Initiative Fund (K.A.K. and M.J.C.) and NASA (K.A.K., M.J.C. and S.S.) under contracts 957652, NSCAT Science Working Team, and NAGW-1666. B.Q. was supported by the Office of Naval Research under contract N00014-92-J-1656. Conversations with R. X. Huang helped clarify the role of heat flux. Geosat altimeter data were provided by NODC, and ECMWF wind data and net surface surface heat flux were provided by NCAR. SST data were processed by RSMAS from the original MCSST product and were made available by the PO-DAAC at JPL. Woods Hole Oceanographic Institution contribution 8975.

## References

- Behringer, D., L. Regier, and H. Stommel, Thermal feedback as a contributing cause of the Gulf Stream, *J. Mar. Res.*, **37**, 699–709, 1979.
- Caruso, M. J., P. J. Flament, Z. Sirkes, and M. K. Baker, Geosat processing tools for analyzing mesoscale ocean features, *Tech. Rept. 90-45*, Woods Hole Oceanogr. Inst., Woods Hole, Mass., 1990.
- Cayan, D. R., Latent and sensible surface flux anomalies over the northern oceans: Driving the sea surface temperature, *J. Phys. Oceanogr.*, **22**, 859–881, 1992.
- Cushman-Roisin, B., On the role of heat flux in the Gulf Stream–Sargasso Sea subtropical gyre system, *J. Phys. Oceanogr.*, **17**, 2189–2202, 1987.
- Davis, R. E., Predictability of sea surface temperature and sea level pressure anomalies over the North Pacific Ocean, *J. Phys. Oceanogr.*, **6**, 249–266, 1976.
- Deser, C., and M. L. Blackmon, Surface climate variations over the North Atlantic Ocean during winter: 1900–1989, *J. Climate*, **6**, 1743–1753, 1993.
- Hogg, N. G., R. S. Pickart, R. M. Hendry, and W. J. Smethie Jr., The northern recirculation gyre of the Gulf Stream, *Deep Sea Res. Part A*, **33**, 1139–1165, 1986.
- Hsiung, J., Estimates of global oceanic meridional heat transport, *J. Phys. Oceanogr.*, **15**, 1405–1413, 1985.
- Huang, R. X., Does atmospheric cooling drive the Gulf Stream recirculation?, *J. Phys. Oceanogr.*, **20**, 751–757, 1990.
- Isemer, H.-J., and L. Hasse, *The Bunker Climate Atlas of the North Atlantic Ocean*, vol. 2, *Air-Sea Interactions*, 252 pp., Springer-Verlag, New York, 1987.
- Kelly, K. A., Comment on "Empirical orthogonal function analysis of advanced very high resolution radiometer surface temperature patterns in Santa Barbara Channel" by G. S. E. Lagerloef and R. L. Bernstein, *J. Geophys. Res.*, **93**, 15,753–15,754, 1988.
- Kelly, K. A., The meandering Gulf Stream as seen by the Geosat altimeter: Surface transport, position, and velocity variance from 73° to 46°W, *J. Geophys. Res.*, **96**, 16,721–16,738, 1991.
- Kelly, K. A., and S. T. Gille, Gulf Stream surface transport and statistics at 69°W from the GEOSAT altimeter, *J. Geophys. Res.*, **95**, 3149–3161, 1990.
- Kelly, K. A., and B. Qiu, Heat flux estimates for the North Atlantic, I, Assimilation of satellite data into a mixed layer model, *J. Phys. Oceanogr.*, **25**, 2344–2360, 1995a.
- Kelly, K. A., and B. Qiu, Heat flux estimates for the North Atlantic, II, The upper ocean heat budget, *J. Phys. Oceanogr.*, **25**, 2361–2373, 1995b.
- Kelly, K. A., and D. R. Watts, Monitoring Gulf Stream transport by radar altimeter and inverted echo sounders, *J. Phys. Oceanogr.*, **24**, 1080–1084, 1994.

- Kushnir, Y., Interdecadal variations in North Atlantic sea surface temperature and associated atmospheric conditions, *J. Clim.*, **7**, 142–157, 1994.
- Large, W. G., and S. Pond, Open ocean momentum flux measurements in moderate and strong winds, *J. Phys. Oceanogr.*, **11**, 324–336, 1981.
- Liu, Z., and H. Yang, The intergyre chaotic transport, *J. Phys. Oceanogr.*, **24**, 1768–1782, 1994.
- Mestas-Nuñez, A., D. B. Chelton, and M. H. Freilich, An evaluation of ECMWF-based climatological wind stress fields, *J. Phys. Oceanogr.*, **24**, 1532–1549, 1994.
- Pierce, S., and T. M. Joyce, Gulf Stream velocity structure through inversion of hydrographic and acoustic Doppler data, *J. Geophys. Res.*, **93**, 2227–2236, 1988.
- Preisendorfer, R. W., *Principal Component Analysis in Meteorology and Oceanography*, 425 pp., Elsevier, New York, 1988.
- Qiu, B., Determining boundary current recirculation gyres from altimetry observations, *J. Geophys. Res.*, **97**, 17,801–17,811, 1992.
- Qiu, B., Determining the mean Gulf Stream and its recirculations through combining hydrographic and altimetric data, *J. Geophys. Res.*, **99**, 951–962, 1994.
- Qiu, B., Variability and energetics of the Kuroshio Extension and its recirculation gyre from the two-year TOPEX mission, *J. Phys. Oceanogr.*, **25**, 2374–2390, 1995.
- Qiu, B., and K. A. Kelly, Upper-ocean heat balance in the Kuroshio Extension region, *J. Phys. Oceanogr.*, **23**, 2027–2041, 1993.
- Qiu, B., K. A. Kelly, and T. M. Joyce, Mean circulation and variability of the Kuroshio Extension from Geosat altimetry data, *J. Geophys. Res.*, **96**, 18,491–18,507, 1991.
- Rhines, P. B., and R. Schopp, The wind-driven circulation: Quasi-geostrophic simulations and theory for nonsymmetric winds, *J. Phys. Oceanogr.*, **21**, 1438–1469, 1991.
- Thompson, J. D., and W. J. Schmitz, A limited-area model of the Gulf Stream: Design, initial experiments, and model-data intercomparison, *J. Phys. Oceanogr.*, **19**, 791–814, 1989.
- Worthington, L. V., On the North Atlantic circulation, *Johns Hopkins Oceanogr. Stud.*, **6**, 110 pp., 1976.
- Wunsch, C., Large-scale response of the ocean to atmospheric forcing at low frequencies, *J. Geophys. Res.*, **96**, 15,083–15,092, 1991.

---

M. J. Caruso, K. A. Kelly, and S. Singh, Department of Physical Oceanography, Woods Hole Oceanographic Institution, Woods Hole, MA 02543. (email: kkelly@whoi.edu)

B. Qiu, Department of Oceanography, University of Hawaii at Manoa, 1000 Pope Road, Honolulu, HI 96822.

(Received April 6, 1995; revised August 4, 1995; accepted August 10, 1995.)